Journal of Structural Geology, Vol. 11, No. 6, pp. 717 to 733, 1989
Printed in Great Britain

0191-8141/89 $03.00 + 0.00

Structural and kinematic evolution of the Teslin suture zone, Yukon: record of an ancient transpressional margin

VICKI L. HANSEN*

Department of Earth and Space Sciences, University of California, Los Angeles, CA 90024, U.S.A.

(*Received* 16 *April* 1988; *accepted in revised form* 12 *February* 1989)

Abstract—The Teslin suture zone (TSZ), Yukon, which forms the fundamental boundary between rocks deposited along the ancient margin of North America, and allochthonous terranes to the west, preserves a complex history of pre-mid-Jurassic convergence and dextral strike-slip translation which is overprinted locally by late Cretaceous dextral strike-slip shear. The TSZ, comprised of a 15–20 km thick structural sequence of ductilely deformed sedimentary and volcanic strata, basalt, peridotite and granitoids, is divisible into distinct elongate structural domains based on the distribution of two well-defined but differently oriented stretching lineations, L_{ds} and L_{ss}. L_{ds} and L_{ss} both formed during non-coaxial ductile deformation; L_{ds} trends E–W and plunges down-dip, whereas L_{ss} trends NNW–SSE and plunges shallowly. Two 1–2 km wide, NNW-trending anastomosing shear zones of L_{ss} cross-cut L_{ds} structures, indicating L_{ss} is younger. Other field relations indicate further that L_{ds} began forming earlier than L_{ss}, followed by a period of coeval L_{ds} and L_{ss} formation; latest motion was dominantly parallel to L_{ss}. Synkinematic mineral assemblages associated with both L_{ds}- and L_{ss}-related structures record greenschist to albite–epidote amphibolite facies conditions.

L_{ds} tectonites record a complex movement history: to the west textural asymmetries indicate west-side-down, or normal shear, whereas in eastern domains top-to-the-east thrust-style asymmetries dominate. L_{ss} tectonites consistently record dextral, or top-to-the-north, shear parallel to L_{ss}. Tectonic motion began as chiefly penetrative dip-slip shear (L_{ds}) at a high angle to the present trend of the TSZ, and evolved to dominantly dextral strike-slip shear (L_{ss}) parallel to the trend of the zone. The geometry, kinematics and sequence of deformation in TSZ tectonites evoke a general model of terrane accretion during oblique plate convergence involving initial shortening at a high angle to the convergent margin and progression to margin-parallel translation.

INTRODUCTION

THE North American Cordillera comprises a mosaic of tectonic terranes accreted to western North America in Mesozoic and Cenozoic time (e.g. Coney *et al.* 1980). Studies of terrane evolution attempt to identify how and where terranes evolved, and when and where they were accreted to North America (Jones *et al.* 1984, see others in Howell 1985), although they rarely address the nature of the accretion process directly. Mechanisms of terrane accretion may be better understood through careful study of zones along which accretion took place—the transition zones between terranes.

The Teslin suture zone (TSZ), southern Yukon, affords us a unique look at the deep-seated portion of one such terrane boundary separating North American strata from accreted terranes to the west (Fig. 1). In this paper I present and discuss detailed structural and kinematic data from penetratively ductilely-deformed rocks of the TSZ within the eastern Laberge–western Quiet Lake map area, northeast of Whitehorse, Yukon (Fig. 1). Rocks of this zone record ductile deformation under moderate- to high-P–T conditions with a tectonic environment of generally E–W convergence; the suture zone progressively evolved from a zone of E–W dip-slip motion, into one of N–S dextral translation under lower-P–T, shallower crustal conditions. The TSZ records the approach of the Yukon–Tanana terrane (YT), and related terranes, to North America and subsequent dextral translation along the early Mesozoic margin prior to final imbrication and emplacement of the YT onto North America in mid-Cretaceous time.

GEOLOGICAL SETTING

Yukon Territory is comprised of several lithotectonic terranes (Fig. 1) (Silberling & Jones 1984). The McKenzie, Selwyn and Cassiar terranes include Proterozoic to Mesozoic continental margin strata of North America. The Yukon–Tanana composite terrane, previously termed the Yukon cataclastic complex (Tempelman-Kluit 1979), and the Yukon crystalline terrane (Tempelman-Kluit 1976, Churkin *et al.* 1982), is an extensive metamorphic–plutonic assemblage exposed over thousands of square kilometers in east-central Alaska and southern Yukon. The YT lies as a thin tectonic flap along its broadest portion east of Fairbanks (Churkin *et al.* 1982), merges with large klippen in southern Yukon and becomes steeply-dipping within the TSZ in central Yukon. The TSZ, defined in the eastern Laberge map area, southern Yukon, is the variably ductilely-deformed, steeply-oriented portion of the otherwise relatively flat-lying YT.

The Slide Mountain terrane (SM), composed of weakly metamorphosed to non-metamorphosed and imbricate thrust slices of oceanic layer 1 strata, rest as klippen, generally east of the YT, on North American miogeoclinal strata in southern British Columbia to

*Present address: Department of Geological Sciences, Southern Methodist University, Dallas, TX 75275, U.S.A.

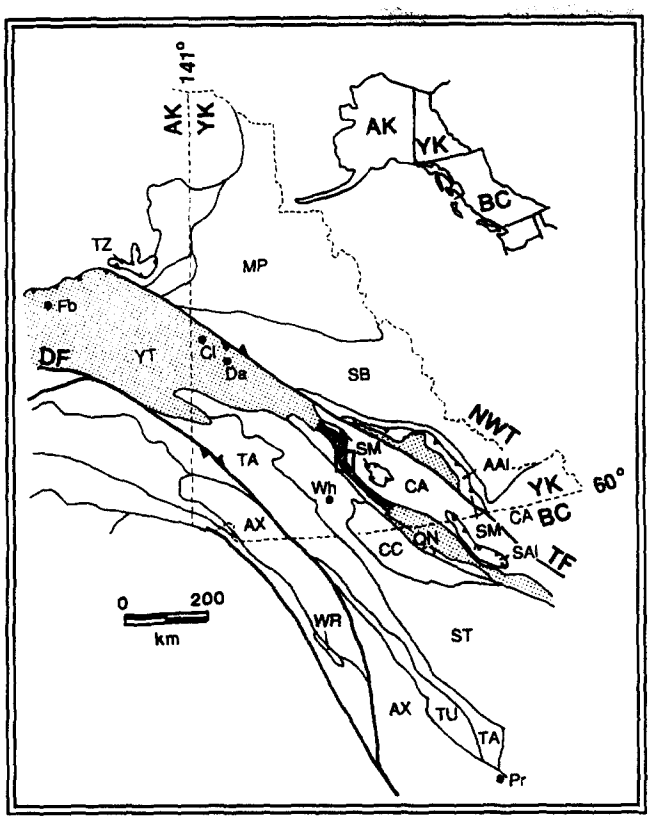

Fig. 1. Tectonic terrane map of Yukon, northern British Columbia and eastern Alaska (modified from Tempelman-Kluit 1979, Jones *et al.* 1984, Monger & Berg 1984). Autochthonous terranes include: CA = Cassiar, MP = McKenzie, SB = Selwyn. Allochthonous terranes include: AX = Alexander, CC = Cache Creek, QN = Quesnel, SM = Slide Mountain (AAI = Anvil allochthon; SAI = Sylvester allochthon), ST = Stikine, TA = Tracey Arm, TU = Taku, TZ = Tozitna, WR = Wrangellia, YT = Yukon–Tanana. Faults include: DF = Denali fault, TF = Tintina fault. Towns include: Cl = Clinton Creek, Da = Dawson, Fb = Fairbanks, Wh = Whitehorse and Pr = Prince Rupert. The Teslin suture zone is the steeply-dipping portion of the YT shown shaded. Box indicates area of Fig. 2. Terranes west of YT are not discussed in this paper.

Alaska (Monger & Berg 1984). The Anvil (usage of Monger & Berg 1984) and Sylvester allochthons of the SM are regionally associated with the YT in northernmost British Columbia and southeastern Yukon (Fig. 1). A low-angle tectonic contact accommodating over 100 km of tectonic overlap juxtaposes the YT and SM against pre-late Jurassic autochthonous continental margin strata in northern Canada; mid-Cretaceous granitic plutons intrude SM and YT thrust sheets, placing an upper limit on terrane emplacement (Tempelman-Kluit 1979). Following emplacement these terranes were displaced along the dextral Tintina fault at least 450 km (Fig. 1) (Roddick 1967, Gabrielse 1986).

The Yukon–Tanana terrane and the Teslin suture zone

The TSZ, so named because it roughly follows the Teslin River in southern Yukon, forms a steeply-oriented, southern prong of the YT in Yukon. The original definition of the TSZ (Tempelman-Kluit 1979) includes both structural and lithologic criteria leading to confusion. I redefine the TSZ in this paper on purely structural, rather than lithologic, grounds. I use the term TSZ to refer to the package of rocks comprising the 15–20 km wide steeply-dipping portion of the YT in southern Yukon (Figs. 1 and 2); these rocks display *L–S* tectonite fabrics indicative of penetrative ductile deformation. The TSZ should not be confused with the Teslin fault, one of a number of discrete, NNW-trending, high-angle brittle faults along the Salmon River valley. Lithologically the TSZ includes units correlative with the YT and with SM assemblages (Hansen 1987b).

The YT and TSZ are divided into five assemblages: metasedimentary and metavolcanic rocks of the Nisutlin and Anvil assemblages, and three granitoid assemblages (Tempelman-Kluit 1979, Mortensen & Jilson 1985, Mortensen 1988). The Nisutlin assemblage, comprised of mylonitic siliceous metasedimentary rocks including white-mica phyllitic quartzite, chlorite–quartz gritstone, calcareous chloritic phyllite to quartzite, graphitic quartzite and phyllite, marble and calcareous schist, may be correlative with YT subterrane Y_3 in Alaska as defined by Churkin *et al.* (1982). Protoliths include Upper Devonian to mid-Mississippian volcanic rocks and Lower Pennsylvanian to early Permian conodont-bearing strata.

The Anvil assemblage includes sheared (garnet–)epidote–mica amphibolite, metabasalt, metamorphosed mafic plutonic and tuffaceous rocks, metachert and minor ultramafic rock. The Anvil assemblage, correlative at least in part with Y_4 of Churkin *et al.* (1982) in eastern Alaska (V. Hansen unpublished mapping), is also lithologically similar to the SM Anvil allochthon, southeast Yukon (Monger & Berg 1984); however, Anvil allochthon rocks do not display penetrative ductile deformation fabrics. Anvil assemblage protolith ages range from the latest Devonian (365–370 Ma, U–Pb zircon from plagiogranite, Mortensen & Jilson 1985) to late Pennsylvanian–early Permian (fossil ages from interbedded sediments, Tempelman-Kluit 1972).

YT granitoids are divided into three assemblages based on lithology, crystallization age, and ^{87}Sr–^{86}Sr and U–Pb systematics (Mortensen 1988). The most widely distributed of these suites includes large bodies of 360–340 Ma (U–Pb zircon) peraluminous orthogneiss, and related metasedimentary rocks, which exhibit extremely high Sr initial ratios and which record an inherited early Proterozoic Pb component (Aleinikoff *et al.* 1981, Dusel-Bacon & Aleinikoff 1985, Mortensen 1985, 1988, Mortensen & Jilson 1985). This assemblage, correlative with Y_1 of Churkin *et al.* (1982) (Dusel-Bacon & Aleinikoff 1985, Mortensen & Jilson 1985), forms the lowest structural level of the YT in Yukon (Mortensen 1988). The Sulphur Creek orthogneiss assemblage, thus far only recognized in west-central Yukon, consists of early Permian gneissic biotite–quartz monzonite and related metavolcanic rocks which show no evidence of inherited Pb. The Simpson assemblage consists of 370–350 Ma (U–Pb zircon) hornblende–biotite–quartz diorite to quartz monzonite with no inherited Pb, and Sr initial ratios of <0.710. Of these three granitoid

assemblages only rocks of the peraluminous orthogneiss assemblage have been positively identified within the study area, although this may be due to the paucity of radiometric data.

The age of metamorphism and ductile deformation within the TSZ and YT is not well known (Foster *et al.* 1987, Dusel-Bacon in press); the YT has a polyorogenic history that is an inevitable source of confusion. This paper, which focuses on the structural evolution of the TSZ, sheds some light on the nature of this polyphase history. Rb–Sr, K–Ar and ^{40}Ar–^{39}Ar cooling ages indicate that major metamorphism and synchronous ductile deformation of TSZ tectonites ended by early Jurassic time (Metcalfe & Clark 1983, Hansen *et al.* in press) as these tectonites were thrust eastward onto North American strata (Hansen 1989). Locally, rocks associated with the YT and adjacent North America record Cretaceous cooling ages (Wilson *et al.* 1985, Armstrong 1988).

This paper focuses on the structural and kinematic evolution of TSZ ductile-deformation fabrics which formed prior to final thrust-style imbrication of the YT with rocks of North America, the constraints these data place on TSZ–YT evolution, and models of terrane accretion.

The eastern Laberge–western Quiet Lake map area (Fig. 2) was targeted for study of the TSZ based on geologic as well as geographic grounds. 1:250,000 maps (Tempelman-Kluit 1977, 1984) provide a regional geologic base, and TSZ lithologic variation provides samples suitable for collateral kinematic and geothermobarometric analysis. Glaciated ridges and valleys trend normal to the structural fabric of the TSZ, permitting efficient data and sample collection along continuous transects. Mapping and sampling along three 0.25–0.5 km wide, 20–25 km long transects (Fig. 2) were chosen on the basis of exposure, previous mapping and spacing. Data collected along these transects provide a structural and petrologic base for an integrated three-part study. (1) Structural and kinematic analysis, the topic of this paper, constrains the movement history of the rocks within this zone. (2) Geothermobarometric analysis of synkinematic metamorphic mineral assemblages, presented in a companion paper (Hansen 1987a and in preparation), places limits on *P–T* conditions during deformation. (3) New geochronometric data (Hansen *et al.* 1988, in press) refine constraints on the temporal evolution of this zone. Over 1000 oriented samples were collected along the three transects from over 400 stations, at a density of five to eight stations per km. Various lithologies were sampled at individual stations in order to optimize application of kinematic and geothermobarometric techniques; although all rocks in the TSZ are ductile tectonites, ~20% of the samples yielded kinematic information.

LITHOLOGIC AND FIELD RELATIONS OF THE TSZ

The TSZ, exposed mostly in the eastern Laberge map area, forms a regionally extensive, subvertical, 15–20 km wide, NNW-trending zone of ductile *L–S* tectonites; to the east the zone flattens and is exposed in klippen with gently-dipping foliation (Fig. 2). *L–S* tectonite fabrics and transposed lithologic contacts characterize the TSZ. West of the d'Abbadie fault contacts parallel foliation and the regional trend of the TSZ. East of the d'Abbadie fault TSZ tectonites lie in klippen comprised of imbricate slices of TSZ tectonites and rest in sharp fault contact with metasedimentary strata below.

Faults and intrusive rocks truncate the TSZ to the south; to the northeast it flattens and merges with the flat-lying YT in Yukon and Alaska. East and north of the study area, open NE-vergent folds and chattermarks on SW-dipping faults indicate NE-directed thrusting of upper-plate YT rocks over lower-plate North American strata (Gordey 1981, Erdmer 1985). Abrupt structural transitions across thrusts of 1 m or less truncate ductile fabrics indicating that thrusting post-dated ductile deformation. To the west, a series of high-angle NNW-trending, post-accretionary faults, including the Big Salmon and Teslin faults, place non-metamorphosed to low-grade volcanic and volcanoclastic sedimentary rocks against higher-grade rocks of the TSZ; little is known of the amount or sense of offset along this set of faults. To the east the high-angle, steeply W-dipping, N-trending d'Abbadie fault disrupts the TSZ. Breccia clasts within the fault zone contain relict ductile fabrics indicating that latest movement along the d'Abbadie fault post-dated earlier ductile deformation.

The TSZ is comprised of mylonitic siliceous and calcareous metasedimentary rocks of the Nisutlin assemblage and mafic metasedimentary and metavolcanic rocks of the Anvil assemblage. Orthogneiss assemblage rocks, originally correlated with autochthonous Upper Proterozoic strata (Tempelman-Kluit 1979), meet all the criteria of the YT peraluminous orthogneiss assemblage (Bennett & Hansen 1988). This package of rocks, though ductilely deformed in a fashion similar to TSZ tectonites, records a very different cooling history from that of TSZ tectonites west of the d'Abbadie fault (and presumably from TSZ tectonites preserved in klippen east of the d'Abbadie fault). They are not considered here as part of the TSZ proper, though the tectonic evolution of these rocks is discussed and places important constraints on models of TSZ evolution.

East of the d'Abbadie fault non-foliated late Cretaceous quartz monzonite plutons (90–75 Ma, K–Ar biotite) (Tempelman-Kluit 1977) truncate orthogneiss assemblage structures and place an upper limit on ductile deformation. Similar plutons also truncate low-angle thrust faults (Tempelman-Kluit 1979).

Structural elements

Rocks of the TSZ display a dynamothermal *L–S* tectonite fabric; foliation dips steeply in the west, and flattens to the east within the TSZ. Metamorphic grade ranges from dominantly epidote-amphibolite facies,

with rare eclogites (Tempelman-Kluit 1970, Erdmer & Helmstaedt 1983) in the west, to greenschist facies in the east. Quantitative geothermobarometric analysis of syn-kinematic mineral assemblages is discussed at length by Hansen (1987a and in preparation), and summarized in this paper together with new geochronometric results (Hansen *et al.* 1988, in press) following the discussion of TSZ structures.

Geologic mapping delineates two coplanar, yet differently oriented, elongation lineations, L_{ds} and L_{ss}, locally marked by rodded quartz, smeared micas and aligned metamorphic minerals. Use of a non-subscripted 'L' in this paper refers to elongation lineation of a non-specific type, and subscripts 'ds' and 'ss' refer to dip-slip and strike-slip types, respectively. L_{ds} and L_{ss} are distinguished in the field, in part, by their trend, and in part by their spatial distribution, as best expressed along the southern transect. Within the western portion of this transect L_{ds}, trends W and plunges down-dip; whereas in the eastern portion of the transect L_{ss}, trends NNW–SSE with shallow plunge. The angle between L_{ds} and L_{ss} remains relatively uniform in the range 60–90° (Fig. 3a). Along the central traverse the angle between L_{ds} and L_{ss} decreases toward zones in which L_{ss} is the dominant, or sole, L (Figs. 3b & c). Individual rock samples may contain both L_{ds} and L_{ss}, although in many cases a single lineation is observed.

Structures geometrically related to L, illustrated in Fig. 4, include: (1) mesoscopic fractures perpendicular to L—most commonly observed in association with L_{ss}, but also locally preserved with L_{ds} (Figs. 3b & c); (2) small-scale, open to isoclinal folds with axes parallel to L and axial planes parallel to mylonitic foliation; (3) fabric asymmetries preserved within the motion plane

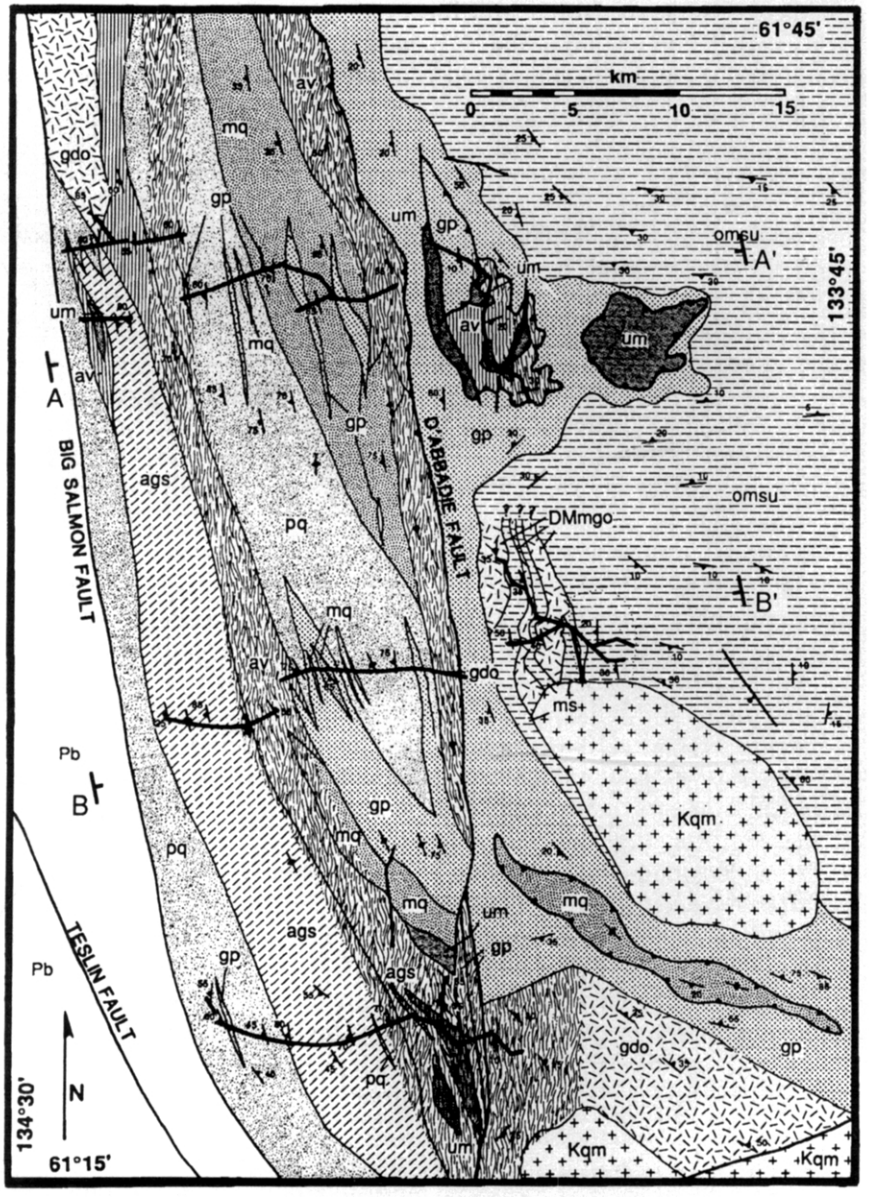

Fig. 2. (a) Generalized geological map of the TSZ within the eastern Laberge–western Quiet Lake map area (modified from Tempelman-Kluit 1977, 1984, Erdmer 1985, Hansen 1987a) Solid lines mark the three transects, northern, central and southern, of this study; cross-section locations shown as A–A′ and B–B′.

(Arthaud 1969) of these tectonites; and locally (4) intersection and crenulation lineations which are generally less well-developed than L and exhibit greater variation in orientation from one plane of schistosity to the next. Small-scale crenulation lineation, present in mica-rich rocks, parallels the local L, with the axial plane generally perpendicular to foliation. These structures, described below, are useful in determining the geometric, kinematic and temporal evolution of L_{ds} and L_{ss}.

L_{ds}–L_{ss} *distribution*

Zones of penetrative L_{ds} and L_{ss} development outline alternating structural domains oriented subparallel to the regional trend of the TSZ (Fig. 2). Transitions from L_{ds} to L_{ss} domains vary from over 10 to 100s of meters. Two zones of L_{ds} formation, the western and central L_{ds} domains, are present in the hangingwall of the d'Abbadie fault, and one, the eastern L_{ds} domain, is present in the footwall. Two zones of strike-slip L are defined within the study area; a western L_{ss} zone bisects L_{ds} domains in the hangingwall, and an eastern L_{ss} zone locally parallels the d'Abaddie fault. Zones of L_{ss} are also interleaved with L_{ds} zones within the klippen along the northern transect.

Deformation along each of these zones was originally interpreted as essentially coeval as no metamorphic hiatus was observed within the tectonite fabrics (Hansen 1986). However, new ^{40}Ar–^{39}Ar data (Hansen *et al.* 1988) differentiate three distinct cooling histories for tectonites within the study area. Hornblende and white-mica from high-P–T hangingwall tectonites yield similar

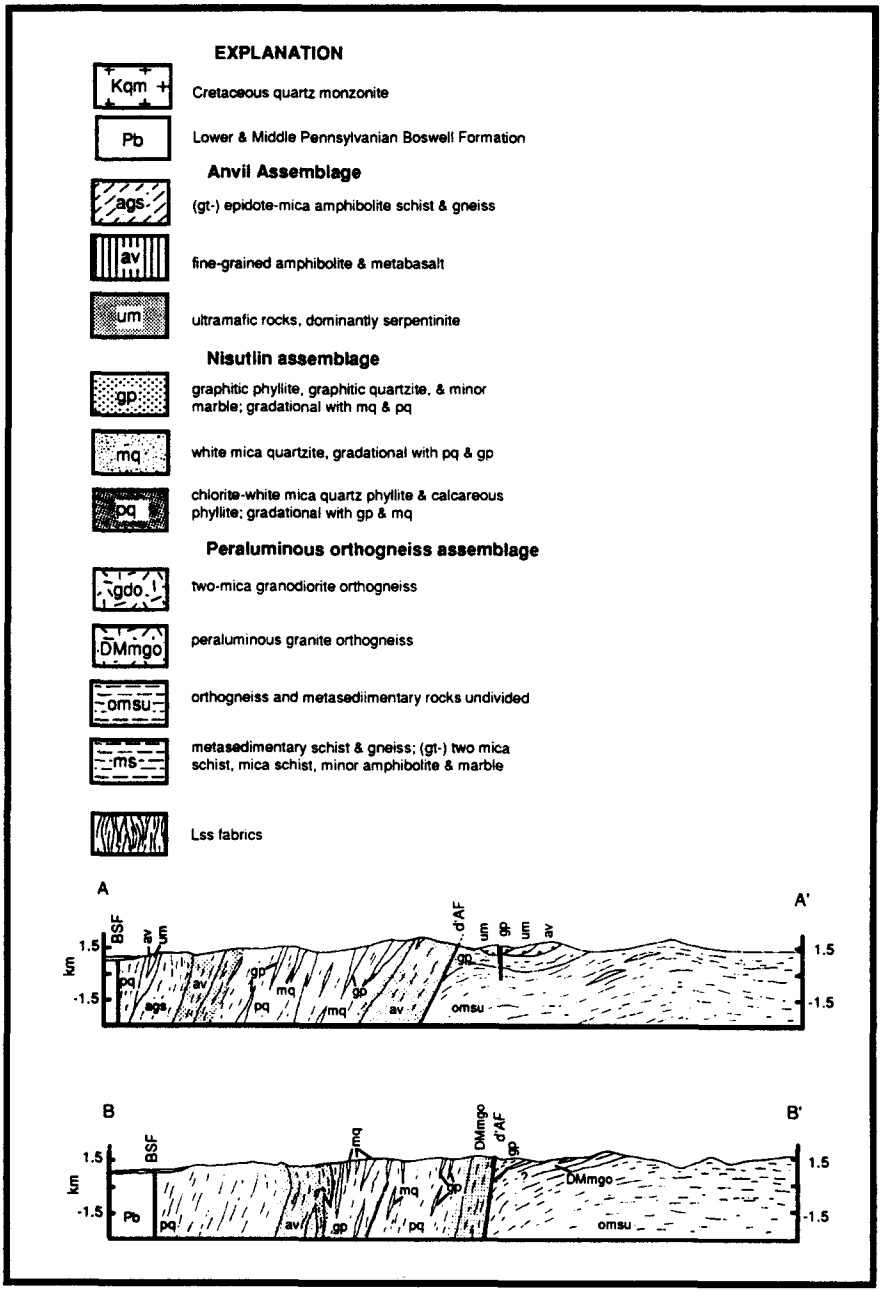

Fig. 2. (b) Geological map explanation and cross-sections A–A′ and B–B′. L_{ss} zones shown in stipple pattern.

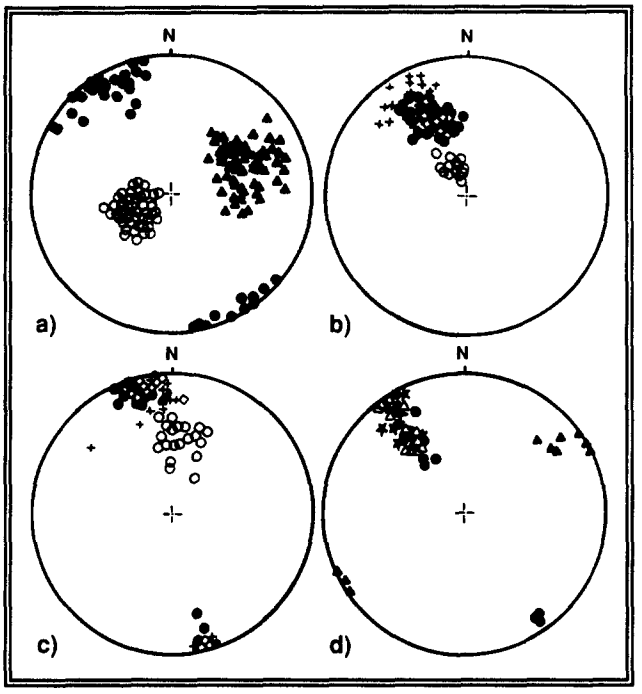

Fig. 3. Lower-hemisphere stereoplots of TSZ structural elements: filled triangles = poles to foliation; open circles = L_{ds}; closed circles = L_{ss}; diamonds = fold axes; crosses = poles to fractures; stars = small-scale folds with interlimb distances of 0.5–2 cm; and open triangles = large folds with interlimb distances of 5–25 cm. Along the southern transect the angle between L_{ds} and L_{ss} is approximately 90° (a); within the central transect the angle between L_{ds} and L_{ss} decreases (b); and L_{ds} shallows in close proximity to a well-developed L_{ss} shear zone along the central transect (c). (d) Angular relations of mesoscopic folds, fractures and L_{ss}.

^{40}Ar–^{39}Ar plateau ages of ~195 Ma (both L_{ds} and L_{ss} fabrics) indicative of extremely fast cooling and calculated uplift rates of ~5 mm a^{-1} assuming a 25°C km^{-1} geotherm. In contrast, hornblende, white-mica and biotite from footwall tectonites (L_{ds}) yield ^{40}Ar–^{39}Ar plateau ages of 150, 118–115 and 110 Ma (1σ errors), respectively. These data indicate slow cooling at ~6°C Ma^{-1} which corresponds to uplift rates of ~0.24 mm a^{-1} assuming a 25°C km^{-1} geotherm. The eastern L_{ss} zone, which locally parallels the d'Abbadie fault, cooled through ~350–300°C by 97 Ma (^{40}Ar–^{39}Ar, mu and bi). Therefore, structural evolution within the hangingwall and footwall, and along the d'Abbadie fault itself must each be considered independently. The hangingwall block includes both L_{ds} and L_{ss} fabrics, whereas the footwall displays L_{ds} fabrics, and ductile fabrics locally parallel to d'Abbadie fault show L_{ss} fabrics. On the basis of ^{40}Ar–^{39}Ar and Rb–Sr data (Hansen *et al.* in press) L_{ds}- and L_{ss}-related shear within the hangingwall occurred during the same tectonic event, and reflect changes in the strain history of this zone. The kinematic evolution of each temporally distinct shear event, and implications of their different cooling histories are discussed in conjunction with tectonic models below.

Timing of fold formation

Parallelism of mineral elongation lineation and minor fold axes is commonly reported from large-scale shear zones (Christie 1963, Eisbacher 1970, Bell 1978, Bell & Hammond 1984), yet mechanisms of fold formation within shear zones are not clearly understood (Platt 1983, Bell & Hammond 1984). In some cases pre-existing, or early-formed, folds rotate into parallelism with the mineral elongation lineation during progressive shear deformation (e.g. Bryant & Reed 1969, Rhodes & Gayer 1977, Bell 1978). Fold rotation during shear deformation implies that folds initiate as open folds with axes at a high angle to the direction of tectonic transport before they rotate into parallelism with L as deformation advances. By this mechanism resultant colinear folds should be tight to isoclinal as a result of continuing shear deformation and overall flattening in the xy plane of the strain ellipsoid.

In contrast, mica-quartzite and augen orthogneiss commonly display open, rather than tight, folds with axes parallel to L (Fig. 3d), indicating that they initiated as open folds with axes parallel to L following, or contemporaneous with, L formation. Thus, they probably did not result from reorientation of pre-existing folds. Additionally, within mylonitic ortho-

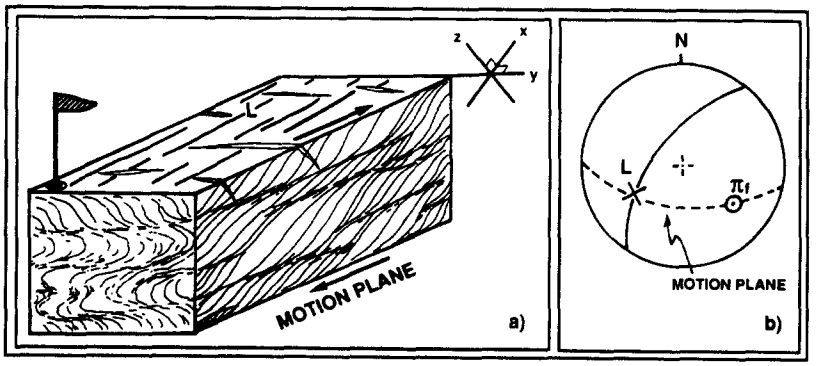

Fig. 4. (a) Stylized block diagram showing typical TSZ tectonic fabric elements including: (1) mylonitic to neoblastic metamorphic foliation, locally comprised of composite *S–C* foliation preserved in the motion plane (Berthé *et al.* 1979); (2) elongation lineation, L; (3) fractures, commonly quartz-filled, perpendicular to L; and locally, (4) open to isoclinal folds with axes parallel to L and axial planes parallel to foliation. (b) Lower-hemisphere stereonet diagram with motion plane (dashed great circle), containing pole to foliation (circle) and L (×).

gneiss (from the eastern L_{ss} domain) the mylonitic foliation is itself folded, indicating that these folds must have initiated *after* the earliest stages of mylonitic foliation development. Therefore, these folds formed either synchronously with, or after the initiation of, penetrative ductile deformation.

Timing of fold formation in these rocks is further constrained by asymmetric fabrics preserved within the motion plane of rocks bearing minor folds. If folding post-dated mylonitization, during which a uniform asymmetric geometry developed, the asymmetry *after* folding would be opposite for each fold limb. This is not the case for TSZ folds, which show interlimb consistency of asymmetric fabric geometry. Therefore TSZ folds must have formed *synchronously* with on-going penetrative, non-coaxial ductile deformation, and apparently nucleated as open-style folds with colinear axes and L. Folds with similar geometric and temporal constraints are described elsewhere (Bell & Hammond 1984, Ridley 1986). Small-scale folds in calcite–mica–quartz phyllite, siliceous phyllite, mica-quartzite and orthogneiss need not record distinct fold events; they are interpreted here to have formed synchronously with ductile deformation. These folds may have formed as a result of strain inhomogeneities or local changes in strain rate during continuous penetrative ductile deformation (Platt 1983). Possible mechanisms by which such folds may initiate are discussed by several authors (Platt 1983, Bell & Hammond 1984, Ridley 1986), although their formation remains problematic.

Relative timing of L_{ds} *and* L_{ss}

Structural relations at several scales help to constrain the relative timing of L_{ds} and L_{ss} formation within the hangingwall of the d'Abbadie fault. At the map scale, L_{ss} zones dissect L_{ds} structural domains. Where L_{ds} is mapped into regions containing L_{ss}, L_{ds} is progressively reoriented into parallelism with L_{ss}. Mesoscopically L_{ss} overprints L_{ds} at locations where they occur together. Rotation of L_{ds} toward L_{ss} is also seen by the reorientation of L_{ds} by open folds interpreted to have formed synchronously with L_{ss}.

Quartz pressure shadows on euhedral pyrite cubes within the foliation plane record progressive change in the orientation of the maximum strain axis from westward dip-slip to north-south strike-slip within the western L_{ss} shear zone (Fig. 5). Antitaxial quartz fibers grow outward from rigid pyrite cubes, reflecting the strain regime during quartz growth (Choukroune 1971). The orientations of the pressure shadow tails indicate that L_{ss} post-dates L_{ds}, and that there was probably a continuous change from the strain regime associated with L_{ds} to that during formation of L_{ss}. Timing relations are further supported by geothermobarometric data which show that L_{ds} hangingwall tectonites record higher P and T metamorphic conditions than adjacent L_{ss} tectonites. These data, summarized below, are discussed more fully in companion papers (Hansen 1987a and in preparation).

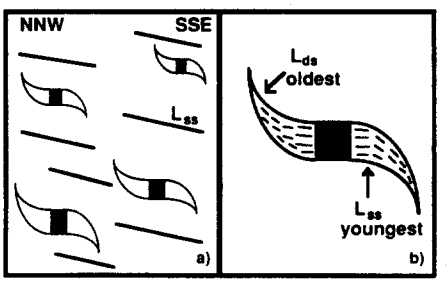

Fig. 5. (a) Quartz strain-shadows on pyrite viewed on a steeply-dipping plane of mylonitic foliation; sample from an L_{ss} shear zone indicates timing relations between L_{ds} and L_{ss}. (b) Quartz fibers grow outward from the pyrite cube and reflect the orientation of incremental principal strain axes during time of crystal growth (Choukroune 1971); L_{ds} is older than L_{ss}. Pyrite cubes are 2–5 mm on a side.

It is possible that dip-slip shear occurred in one region of the TSZ while strike-slip shear occurred elsewhere within the TSZ. However, L_{ss} formation dominantly outlasted formation of L_{ds}, indicating that penetrative dip-slip shear gave way progressively to localized strike-slip shear.

Kinematic interpretation of L_{ds}–L_{ss} *fabrics*

Fabric asymmetry within the motion plane (Fig. 4) of TSZ tectonites records the sense of tectonic transport during ductile deformation. Useful kinematic indicators include: macroscopic and microscopic asymmetric folds with axes normal to L, rotated clasts, shear bands, S–C fabrics, and microscopic mica fish, quartz pressure shadows on pyrite, quartz grain-shape preferred orientation, quartz lattice preferred orientation and rare rotated garnets.

Although kinematic interpretation of microstructures is an extremely valuable tool in structural analysis, it is a difficult science to quantify. Short of presenting a photograph and detailed discussion of each thin section, it is difficult to evaluate the quality of a study which relies on detailed kinematic analysis. In addition to difficulties in objectivity and quantification, problems arise in kinematic analysis because some microstructures are more consistently interpretable than others; furthermore, many lithologies do not develop, or preserve, structures useful for kinematic analysis. Such difficulties may not present problems within shear zones which have a simple strain history, however, such factors should be considered in study of zones, such as the TSZ, which record complex strain histories.

In order to address these concerns, I examined thin sections representing each lithology present at any one station, and devised a numerical scale to provide a measure of confidence in the kinematic interpretation made at a given sample station. The reliability index is based on the type of kinematic indicator, the clarity or intensity of development of the asymmetric fabric, and the number of different kinematic indicators preserved within samples from a single station. The reliability index ranges from 0 to 5. Ratings of 4 and 5 are trustworthy, whereas a rating of 1 means a potentially

ambiguous interpretation was made; 0 represents no kinematic interpretation. It is difficult to establish an absolute confidence scale in order to compare kinematic interpretations among researchers; however, the reliability index employed in this study allows the reader to compare the 'quality' of kinematic interpretations throughout the TSZ.

Asymmetric motion plane structures visible in the field are relatively rare; yet, asymmetric folds and rotated silica-rich boudins yield consistent shear sense in impure marble, and shear bands and *S–C* fabrics commonly are well-developed in peraluminous orthogneiss. Many TSZ rocks are fine-grained, however, and field examination does not permit trustworthy kinematic determinations; hence, oriented samples were examined in thin section.

Type I *S–C* fabrics (Lister & Snoke 1984), best preserved within the eastern L_{ss} zone, are interpreted with confidence in thin section (Fig. 6a) and rate 5 on the reliability index; shear sense is consistent with field interpretation. The form and orientation of mica fish (locally partially recrystallized) in type II *S–C* fabrics (Lister & Snoke 1984) in mica quartzite and (garnet–)epidote–mica amphibolite (Fig. 6b) west of the d'Abbadie fault and in peraluminous orthogneiss east of the d'Abbadie fault provide evidence of pre-annealing, non-coaxial deformation, and shear sense in rocks in which quartz grains are equant and annealed. Quartz pressure shadows on pyrite cubes in pyrite–chlorite–mica phyllite (Fig 6c) show fabrics with consistent asymmetries. Quartz fibers record maximum infinitesimal strain. Locally, complex pressure shadows associated with rotated pyrite cubes (Fig. 7a) may allow minimum estimates of incremental and finite strain values (Etchecopar & Malavieille 1987).

Composite foliation asymmetry, marked by compositional layering and quartz grain-shape preferred orientation, is an indication of non-coaxial deformation and records shear sense (Fig. 7b). Similarly, detrital quartz grains in mica-quartzite commonly are elongate and inclined to the mesoscopic foliation marked by mica. These grains may be treated as qualitative strain markers, indicating both a non-coaxial component of deformation and a sense of shear (Fig. 7c). One sample displays well-developed snowball garnets, and, although opposite senses of shear are recorded within the thin section of this sample, dominant shear sense is consistent with that interpreted in adjacent samples.

Quartz *c*-axis fabric diagrams of TSZ tectonites (Fig. 8) provide evidence that *L* is an elongation lineation as fabric girdles intersect the foliation normal to *L* (Behrmann & Platt 1982). Quartz *c*-axis fabric asymmetry (Figs. 8b–h) indicates non-coaxial shear sense, whereas a lack of fabric asymmetry (Figs. 8a & i) suggests a dominant component of coaxial deformation (Lister & Williams 1979, Schmid & Casey 1986).

Kinematic interpretations and relative levels of confidence of tectonite fabrics are summarized in Fig. 9. Both L_{ss} zones, though differing in their age of formation, consistently record right-lateral, or top-to-the-north (easternmost portion of the southern transect), shear parallel to L_{ss}. Tectonic shear associated with L_{ds} is more complex. Within the hangingwall block the western L_{ds} domain consistently records west-side-down (normal) dip-slip displacement. However, within the central L_{ds} domain, also of the hangingwall block, west-side-up (reverse) dip-slip shear is more common, although microstructures indicating normal movement are also present. Within the eastern L_{ds} domain of the footwall top-to-the-east shear is recorded along the central transect. Microstructures are better developed, or preserved, within the western L_{ds} domain than in the central and eastern L_{ds} domains; as a result, kinematic interpretations are generally at higher levels of confidence in the western L_{ds} domain. Consistent fabric asymmetry and more strongly developed fabrics within the western domain may indicate a greater component of simple shear-dominated deformation during L_{ds}. It is also possible that this region escaped later fabric annealing or later coaxial flattening. With no quantitative strain determinations each of these interpretations is permissible.

Nisutlin and Anvil rocks within the klippen east of the d'Abbadie fault record reverse movement parallel to L_{ds} and right-lateral, or top-to-the-north, shear parallel to L_{ss}.

Structural and kinematic evolution

Geometric, kinematic and temporal data which constrain the polyphase tectonic evolution of the TSZ and adjacent rocks are summarized in a schematic block diagram (Fig. 10). L_{ss} tectonites, spatially associated with, but cut by, the d'Abbadie fault record dextral strike-slip shear which ended by late Cretaceous time (98–97 Ma, ^{40}Ar–^{39}Ar mu & bi) (Hansen *et al.* 1988). This zone, together with the d'Abbadie fault, separate tectonite packages with different movement and cooling histories. Hangingwall rocks record moderately high-*P*–*T* pre-early Jurassic dip-slip and strike-slip ductile shear, whereas footwall rocks record late Jurassic to mid-Cretaceous top-to-the-east ductile shear.

Hangingwall tectonites evolved in a zone of moderately high strain; deformation within this zone is at least in part non-coaxial in character. Lithologies incorporated in the zone were juxtaposed prior to, or synchronous with, movement and associated non-coaxial strain. Tectonic movement began as coherent dip-slip motion at a high angle to the trend of the zone of deformation, and evolved to right-lateral translation parallel to the trend of the zone along discrete 1–3 km wide shear zone(s). High-*P*–*T* crustal conditions accompanied initial dip-slip deformation, which evolved, at lower crustal conditions, into zones of dextral strike-slip translation. Geothermobarometric studies provide evidence that high-*P*–*T* metamorphism of the TSZ occurred within a coherent belt at least 10–15 km wide and greater than 60 km long. Eclogite, structurally enclosed by TSZ tectonites, records high-*P* metamorphic conditions at depths greater than 40 km

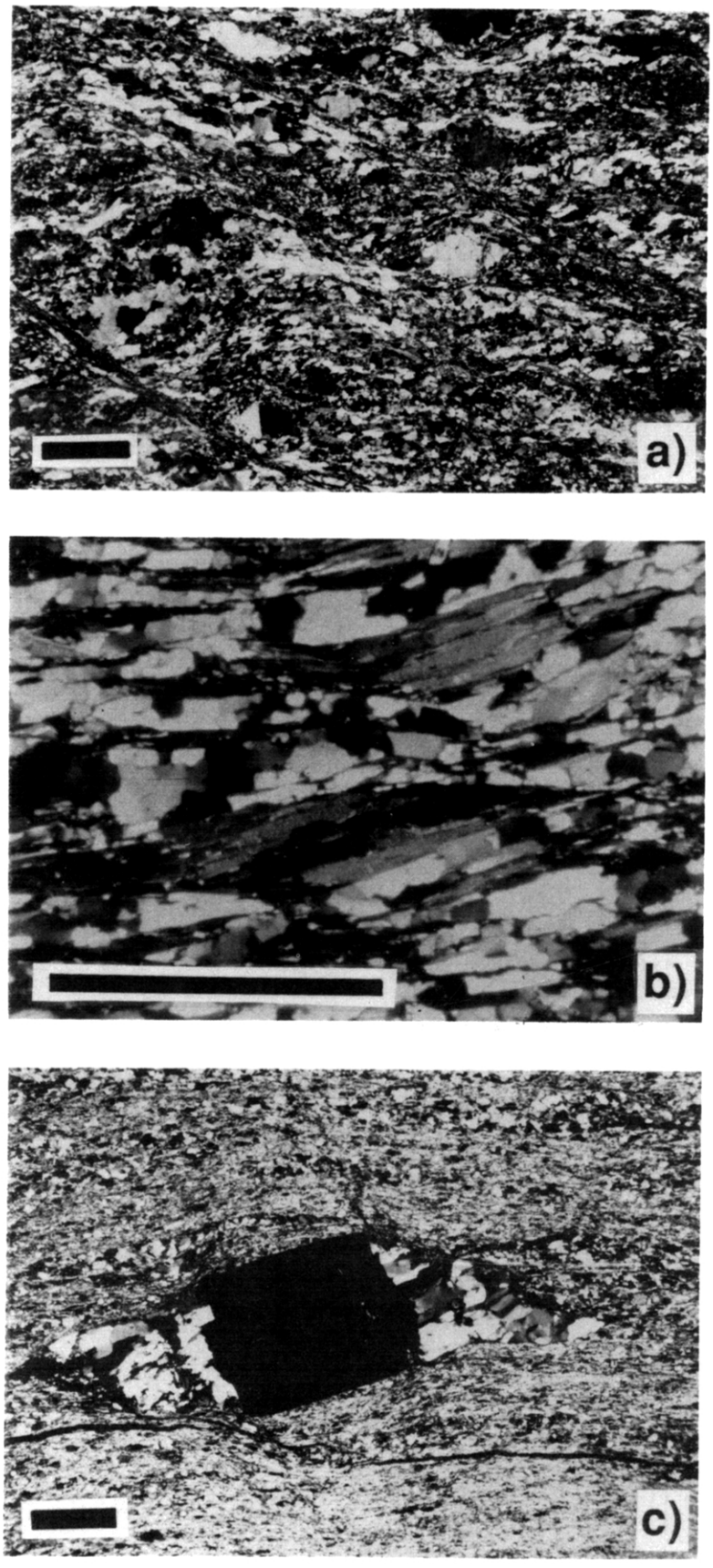

Fig. 6. Kinematic indicators useful for TSZ rocks: (a) *S–C* fabrics with *S* subhorizontal and *C* trending downward to the right; (b) mica 'fish' (note flat field extinction of quartz); (c) asymmetric quartz strain shadows on pyrite. All photographs lie in the *xz* plane and indicate dextral displacement; black bar = 1 mm.

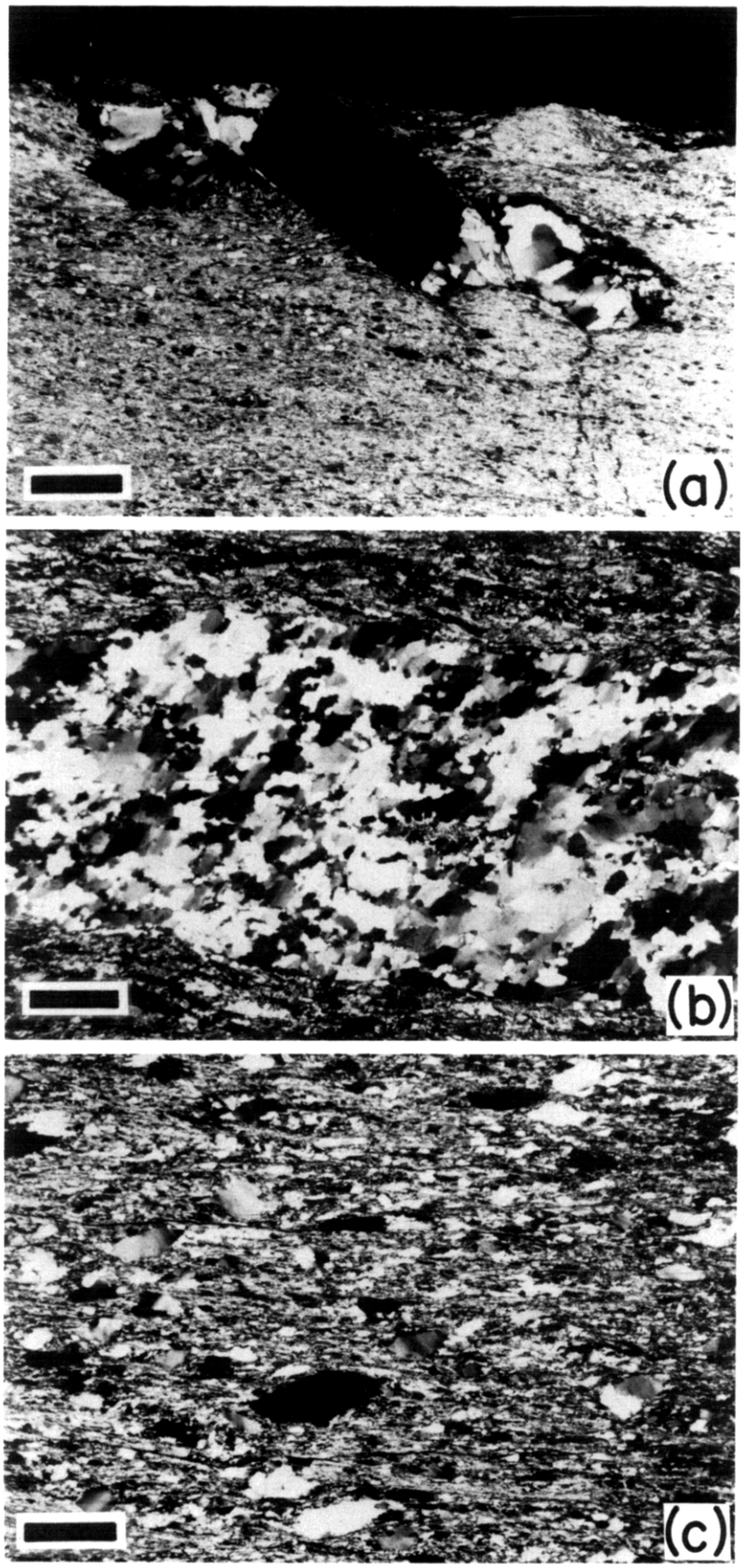

Fig. 7. Kinematic indicators useful for TSZ rocks: (a) quartz strain shadow on rotated pyrite cube indicates sinistral displacement; (b) obliquity of flattened quartz grains with respect to macroscopic foliation marked by very fine-grained mica indicates dextral displacement; and (c) elongate detrital quartz inclined to the mesoscopic mylonitic foliation in mica quartzite indicates dextral displacement. All photographs lie in the *xz* plane; black bar = 1 mm.

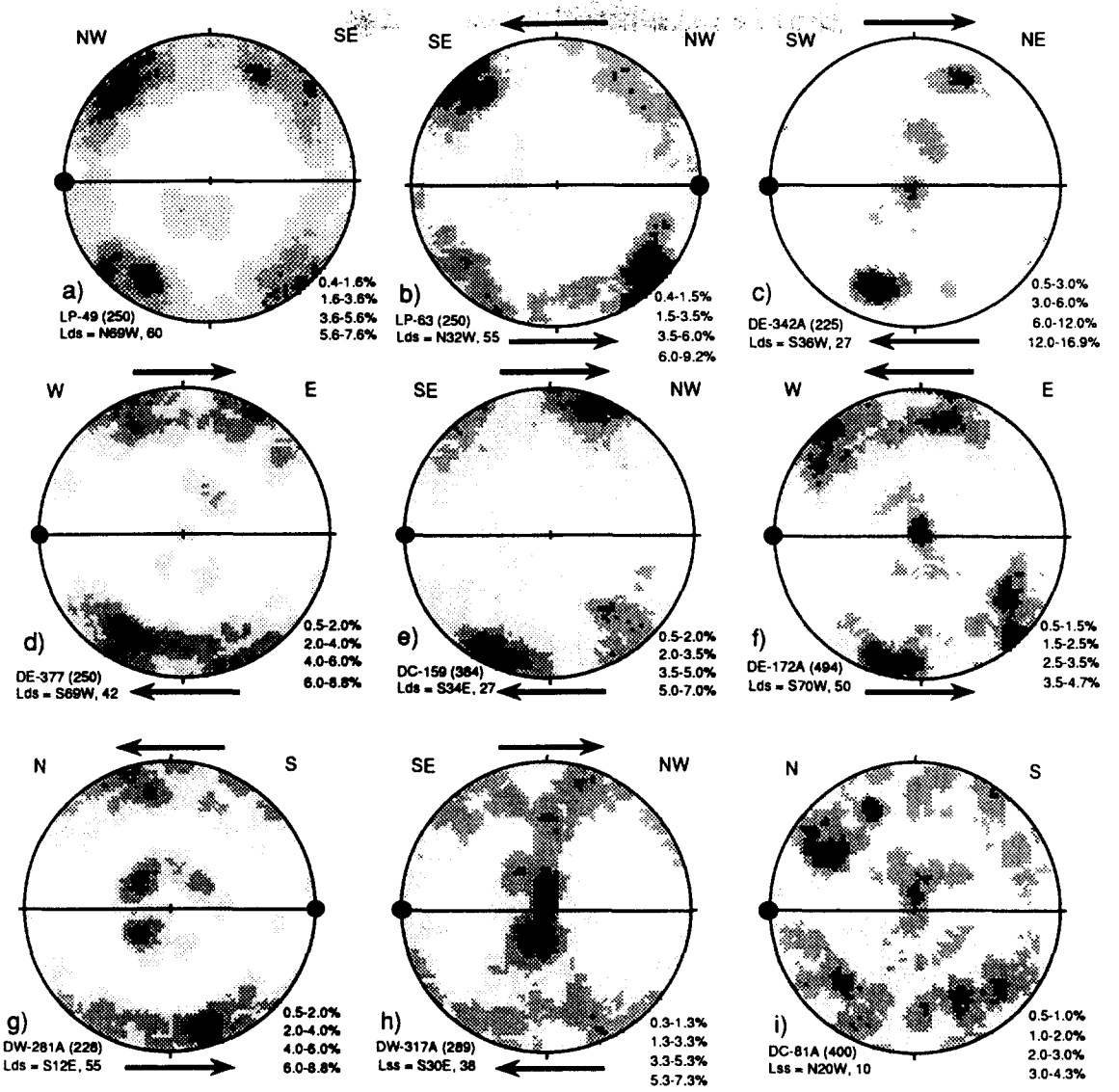

Fig. 8. Quartz *c*-axis fabric diagrams of TSZ tectonites measured in the *xz* principal plane, normal to foliation and containing *L*, using standard universal stage techniques (Turner & Weiss 1963, pp. 197–203). Stereoplots are oriented with respect to *L*; horizontal solid lines mark foliation (*S*), and dots represent down-plunge *L* orientation. Approximate geographic co-ordinates are shown above each stereoplot. The number of *c*-axes is shown in parentheses next to the sample number. Pole-free area is white and pole maxima are black; density contours for each sample are given in per cent per 1% area. (a) LP-49E, L_{ds} graphitic quartzite; (b) LP-63, L_{ds} graphitic quartzite; (c) DE-342A, L_{ds} quartzite with minor muscovite; (d) DE-377, L_{ds} quartzite with minor muscovite; (e) DC-159, L_{ds} quartzite; (f) LV-172 L_{ds} quartzite; (g) DW-281A, L_{ss} quartzite; (h) DW-317C, L_{ss} quartzite; and (i) DC-81A, L_{ss} quartzite layer in amphibolite. Sample locations shown in Fig. 9. Kinematic interpretations are shown with each stereoplot.

(Erdmer & Helmstaedt 1983); the enclosing tectonites also record high-*P*–*T* metamorphic conditions (575–675°C and 8–16 kbar, Hansen 1987a and in preparation). Initial, regionally penetrative, high-*P*–*T* dip-slip shear progressively evolved into strike-slip shear at lower *P*–*T* conditions (425–550°C and 5–8 kbar) (Hansen 1987a and in preparation) and hence shallower crustal levels. Hangingwall rocks record extremely fast cooling in early Jurassic time, whereas footwall rocks, which record top-to-the-east ductile shear and amphibolite grade metamorphism, cooled slowly in late Jurassic to mid-Cretaceous time.

Within the hangingwall tectonites normal dip-slip shear is recorded to the west of the dextral shear zone and dominantly reverse dip-slip shear is recorded to the east. This record of both normal and reverse movement parallel to L_{ds} cannot be the result of post-kinematic folding of L_{ds} fabrics during NE-directed thrusting. Formation of NE-vergent folds, with axes at a high angle to L_{ds}, during thrusting would not result in an apparent reversal of shear; rather, tight folds of this orientation would repeat the structural section retaining similar shear sense throughout. Therefore, models for pre-early Jurassic TSZ ductile deformation must consider both normal and reverse motion parallel to L_{ds}, with normal shear preserved to the west and dominantly reverse shear to the east. In addition, models must explain a change from dip-slip shear under moderately high-*P*–*T* conditions to dextral strike-slip shear at lower *P*–*T* conditions.

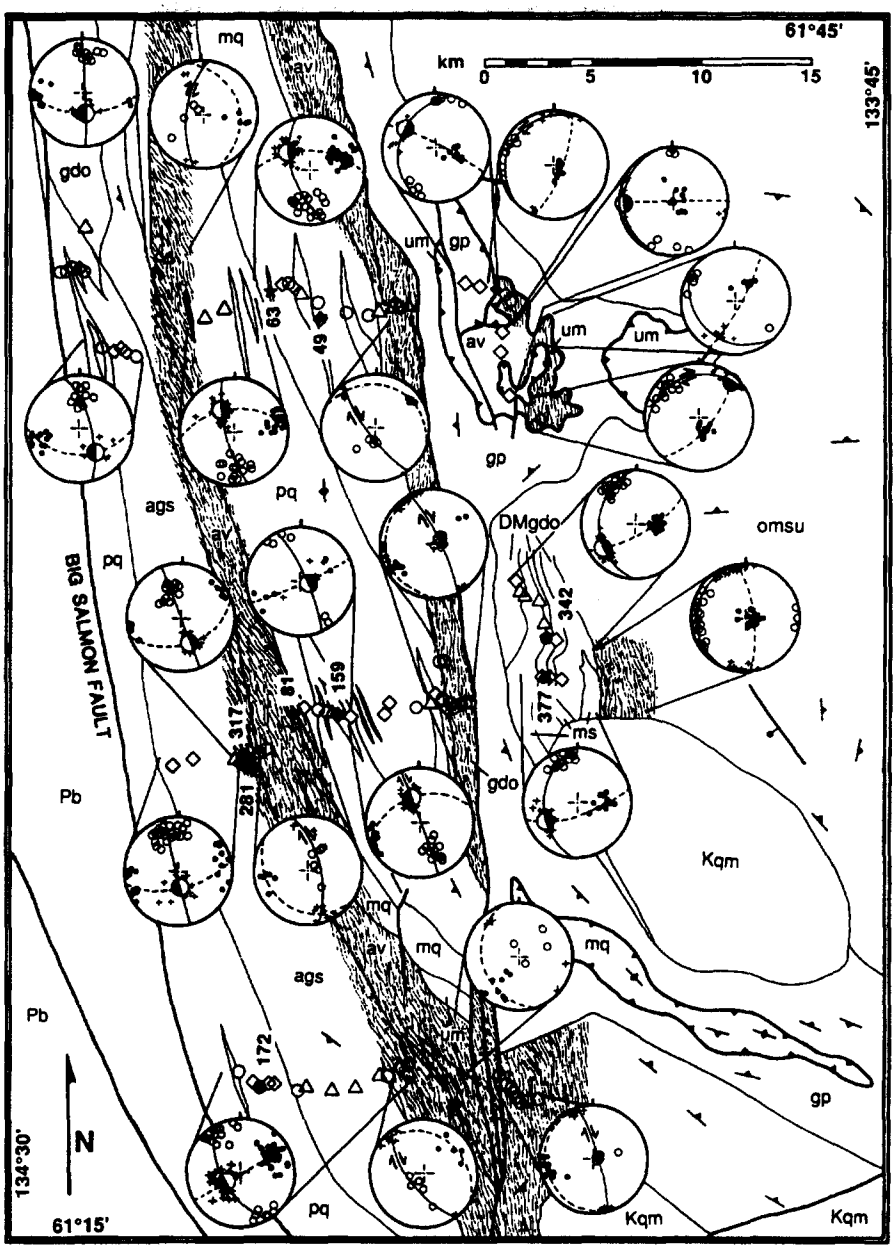

Fig. 9. Compilation of TSZ kinematic interpretations. Lower-hemisphere stereoprojections show poles to foliation (○), *L* (+) and poles to motion planes (●). Average foliation planes are shown as solid lines, and average motion planes are shown as dashed lines. Arrows show relative direction of strike-slip translation component. Large split circle symbols indicate relative dip-slip component of shear; filled half marks down-dropped side. Sample locations for quartz *c*-axis fabric patterns are labeled with numbers. Location of other samples are shown by symbols along each transect; symbol type represents reliability index of kinematic interpretation: △ = 1–2; ◊ = 3; ○ = 4–5. See text for explanation.

Following dip-slip and strike-slip dynamothermal deformation (or during the latest stages of deformation) hangingwall tectonites were uplifted and cooled quickly (~50°C Ma^{-1}) through at least 300°C in early Jurassic time. In contrast, footwall peraluminous orthogneiss assemblage rocks, which record top-to-the-east thrust(?)-style shear, cooled slowly (~5°C Ma^{-1}) during late Jurassic to mid-Cretaceous time. Locally tectonites similar to those west of the d'Abbadie fault lie in klippen structurally above peraluminous orthogneiss east of the d'Abbadie fault. Sharp faults which bound these klippen are constrained as post-ductile deformation, hence post-195 Ma; top-to-the-east movement along these faults (Erdmer 1985) is consistent with similar faults outside the study area (Gordey 1981). Field relations outside the field area also indicate that displacement along similar faults pre-dates the emplacement of mid- to late Cretaceous plutons (Tempelman-Kluit 1979).

Uplift rates of ~5 mm a^{-1} calculated for hangingwall tectonites (assuming a 25°C km^{-1} geotherm) are similar to those determined for Himalayan Pliocene uplift (Copeland *et al.* 1988) and are interpreted to result from rapid uplift associated with E-directed thrusting (Hansen submitted). In contrast, uplift rates of ~0.24 mm a^{-1} (assuming a similar geotherm) calculated from orthogneiss assemblage metasedimentary strata east of the d'Abbadie fault are consistent with erosion rates.

Footwall orthogneiss and related metasedimentary

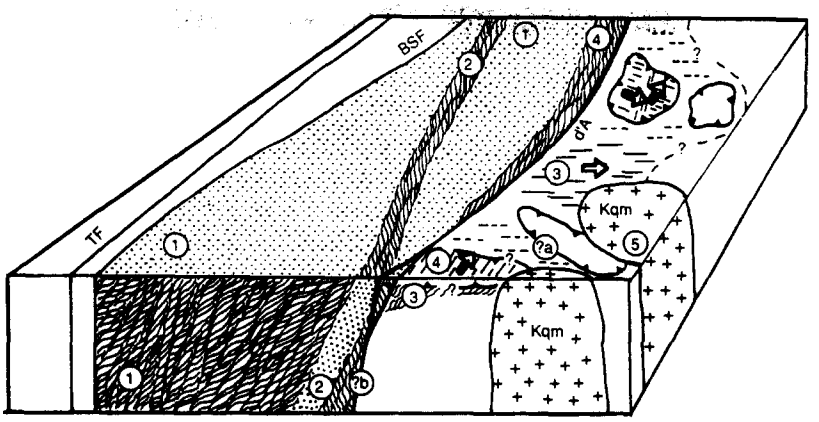

Fig. 10. Schematic block diagram illustrating structural and kinematic domains, and geometric, kinematic and temporal constraints on the tectonic evolution of the TSZ and adjacent rocks; compare with Figs. 2 and 9. Shear pattern marks the approximate orientation of the motion plane for each structural domain with asymmetry illustrating dominant shear sense; stippled areas are approximately normal to the motion plane and to the direction of tectonic transport (L). Line pattern is approximately parallel to L within the foliation plane, lines are dashed where deformation is inferred, open arrows indicate approximate direction of displacement of the upper plate. 1–5 indicate the relative order of events. 1 and 2 are pre-early Jurassic and show quick cooling by ~195 Ma; 3 preceded or was synchronous with slow cooling from 150 to 110 Ma; 4 cooled through 350–300°C by 97 Ma; 5 intruded in mid- to late Cretaceous time. 4 and 5 may have locally occurred synchronously. $?_a$ probably predated intrusion of 5, although this is not constrained within the map area; $?_b$ must post-date 4, but it's relationship with respect to 5 is unconstrained. BSF = Big Salmon fault; TF = Teslin fault; d'AF = d'Abaddie fault. Lithologic symbols are those used in Fig. 2.

rocks, originally correlated with North American Paleozoic strata on the basis of lithology and field relationships (Tempelman-Kluit 1977), can also be correlated with the YT peraluminous assemblage on the basis of lithology, as well as U–Pb, Sm–Nd and ^{87}Sr–^{86}Sr isotopic data (Bennett & Hansen 1988, Mortensen 1988). These rocks, and perhaps others of the YT peraluminous assemblage, may thus be autochthonous North American strata. Preservation of YT peraluminous orthogneiss in the lowermost structural levels of the YT (Mortensen 1988) is consistent with this interpretation.

Hangingwall tectonites may have been thrust over footwall tectonites in early Jurassic time. As a result of thrusting hangingwall rocks cooled quickly, whereas footwall rocks were tectonically buried, insulated from rapid conductive heat loss, and hence *not* cooled during E-directed thrusting. In such a scenario, footwall rocks cooled only during later exposure by uplift or erosion.

Following uplift of these footwall rocks, and related strata along the northern Cordillera, the region was sheared in a dextral sense along high-angle faults and intruded by mid- to late Cretaceous plutons. Upper crustal movement along high-angle faults marked by brittle deformation, such as the d'Abbadie, Big Salmon and Teslin faults, further disrupted the area. The sense of displacement along the high-angle of the d'Abbadie, Big Salmon and Teslin faults is unconstrained. Movement along the d'Abbadie fault must post-date late Cretaceous dextral strike-slip ductile shear. Late Cretaceous quartz monzonite plutons locally cross-cut the d'Abbadie fault; however, crystallization ages are poorly constrained by K–Ar biotite ages ranging from 91 to 75 Ma (Tempelman-Kluit 1984). Movement along the Big Salmon and Teslin faults must post-date pre-early Jurassic ductile deformation; Upper Cretaceous andesite flows and breccia locally overlie these faults (Tempelman-Kluit 1984) placing an upper limit on the time of displacement.

MODELS OF TSZ EVOLUTION

Previous petrotectonic models

Two quite different models of YT tectonic evolution have been proposed to explain penetrative pre-accretion ductile deformation within the YT and TSZ. Tempelman-Kluit (1979) asserted that the whole of the YT represents ductilely-deformed trench-mélange materials (Nisutlin assemblage) formed within an ancient W-dipping subduction complex beneath an E-facing arc (Simpson assemblage) during closure of a broad ocean basin (Anvil assemblage). Within the TSZ rocks of each assemblage were tectonically juxtaposed, deformed and metamorphosed. Following cessation of subduction, these rocks were imbricated and emplaced on North American strata in mid-Jurassic to mid-Cretaceous time. By contrast, workers in Alaska and southeastern Yukon propose that YT ductile deformation and associated metamorphism resulted from widespread emplacement of Paleozoic plutons; these workers suggest that the YT may represent a Paleozoic arc terrane which has been imbricated and accreted to North America (Dusel-Bacon & Aleinikoff 1985, Mortensen 1985, Mortensen & Jilson 1985, Nokleberg & Aleinikoff 1985, Aleinikoff *et al.* 1986).

These two models of YT tectonic evolution by subduction–accretion or arc imbrication differ in three major respects: kinematic evolution, timing and P–T conditions of dynamothermal metamorphism. The two models do not disagree on the time or sense of vergence associated with final imbrication and emplacement of the YT onto North America.

Structural and kinematic data from the eastern Laberge–western Quiet Lake map area does not support, nor allow, a model which requires that TSZ ductile deformation results from intrusion of late Paleozoic plutons, the orthogneiss assemblage. If ductile deformation resulted from pluton emplacement deformation should increase toward plutons, igneous rocks should be most strongly deformed near their borders and less deformed toward their cores, structures in the country rocks should conform to pluton margins, and the metamorphic grade of the country rocks should increase toward the plutons. However, within a TSZ neither structural fabrics nor metamorphic facies show any correlation with the orthogneiss bodies. Within the TSZ deformation intensity shows no correlation with orthogneiss distribution, orthogneiss bodies are elongate parallel to the trend of regional structures within TSZ but they do not define it, and other than a general eastward decrease in metamorphic grade, the major variation in P–T conditions correlates with L_{ss} shear zones rather than orthogneiss. In addition, geothermobarometry of TSZ rocks indicates high-P–T synkinematic metamorphic conditons, not low-P–T conditions expected during pluton emplacement-related metamorphism. Isotopic constraints also indicate that pervasive dynamothermal metamorphism ended, cooling quickly, by early Jurassic time. These relationships indicate that penetrative ductile deformation and associated metamorphism of the TSZ could not be related to the intrusion of Paleozoic plutons.

I propose a model of TSZ evolution conceptually similar to the model proposed by Tempelman-Kluit (1979) although the structural and kinematic data presented herein allow proposal of a more detailed kinematic model with important differences. Coherent and regionally extensive high-P–T conditions recorded by L_{ds} tectonites are consistent with convergent-margin tectonism and are interpreted as having formed within a subduction zone environment. The general eastward decrease in metamorphic grade suggests that the TSZ evolved within a W-dipping (present co-ordinates) subduction zone.

Character of the ancient TSZ subduction complex

Materials incorporated into the subduction complex included pelagic marine sediments, mafic ocean crust and depleted(?) upper mantle and, perhaps locally, components of a magmatic arc. Upon metamorphism and deformation within the subduction zone, these protoliths formed three principal assemblages: (1) most siliceous metasediments, including metachert, carbonate–mica quartzite, graphitic phyllite and minor marble; (2) mafic and ultramafic rocks, consisting of metabasalt, eclogite and serpentinite; and (3) metamorphosed magmatic rocks of intermediate composition, including orthogneiss and metavolcanic rocks. Rocks of each of these lithotectonic assemblages were complexly deformed under high-P–T metamorphic conditions.

Unlike brittlely deformed mélange (Cowan 1985), TSZ rocks exhibit geometrically and spatially coherent ductile structures. Units which form elongate lenses parallel to foliation and the trend of the TSZ are complexly interleaved with one another. Contacts are penetratively ductilely deformed and transposed. Although there is evidence of faulting synchronous with ductile deformation, rocks reflect dominantly macroscopic and mesoscopic ductile deformation.

Ductile-style TSZ deformation is compatible with calculated metamorphic temperatures. Temperature are higher than those typically inferred for blueschist terranes indicative of subduction zone tectonics; yet, average L_{ds} P–T estimates record a low geothermal gradient ($\sim$16°C km^{-1}) compatible with a subduction environment. TSZ rocks may have been deformed close to the overriding plate in the uppermost part of a subduction zone, and they represent a sequence of highly deformed rocks underplated to the hangingwall of an ancient subduction complex.

Material incorporated into the subduction channel can be underplated onto the hangingwall either during downflow or return flow within the subduction channel (Cowan & Silling 1978, Cloos 1982, Shreve & Cloos 1986), and hence provide a mechanism to generate both normal and reverse dip-slip tectonism. The western L_{ds} domain of the TSZ, which records apparent normal movement, could have been underplated to an overriding arc hangingwall at relatively deep crustal levels during subduction return flow. Similarly, the central L_{ds} domain, which records both normal and reverse dip-slip displacement, may preserve a record of return flow and downflow, respectively, as materials were underplated to the overriding arc. Such a model explains the differential dip-slip displacement recorded within the TSZ.

The western L_{ss} domain bisects the western and central L_{ds} domains of the TSZ. Although movement within the western L_{ss} zone dominantly outlasted dip-slip motion within the western and central L_{ds} zones, dip-slip *and* strike-slip motion may have been occurring synchronously, or alternately, prior to final uplift of the TSZ; TSZ structures provide, in general, a single snapshot of the kinematic evolution of the TSZ. Rocks deformed in the western L_{ss} zone record lower metamorphic conditions than hangingwall L_{ds} tectonites, indicating that L_{ss} shear zone formed at higher crustal levels than tectonite fabrics associated with dip-slip tectonics. L_{ss} shear progressively evolved from high-P–T dip-slip deformation, and may, therefore, represent deformation within subduction-related strike-slip shear zones.

Beck (1986) modeled subduction-related strike-slip faults in areas of oblique plate convergence and predicted that ancient subduction complexes may preserve a record of such shear zones. Evidence for subduction-related strike-slip faulting in upper crustal rocks (Fitch 1972, Karig *et al.* 1986) and mid-crustal rocks (Toriumi & Mausi 1986) has been described in the literature. Beck (1986, fig. 4) represents subduction-related strike-slip faults as vertical faults truncated against the interplate

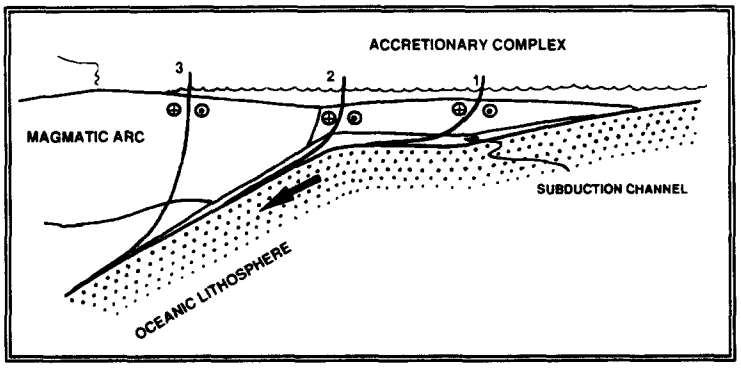

Fig. 11. Schematic diagram showing a continental arc being dismembered by subduction-related strike-slip faults during oblique convergence; diagram is modified from Beck (1986, fig. 4) to show high-angle strike-slip faults at the surface shallowing at depth into the zone of décollement between the two plates—that is, the subduction channel. Circled dots and crosses indicate motion out of and into the plane of the diagram, respectively.

décollement; however, strike-slip faults, which are high-angle near the surface, probably shallow at depth and root into the mechanically weakened décollement of the subduction zone (Fig. 11). In a simple case of oblique subduction as shown in Fig. 11, the strike-slip faults evolve with listric geometry dipping toward the arc as required by convergence direction.

As subduction beneath the overriding arc terrane continues synchronously with margin-parallel translation, early-formed strike-slip shear zones may be progressively overprinted by dip-slip motion during continued plate convergence. Therefore, one might expect preserved portions of a ductilely-deforming subduction complex to record dip-slip motion, overprinted by the later-preserved shear zones related to lateral translation. Margin-parallel shear zones finally preserved in the rock record will have formed at higher crustal levels in general than the dip-slip shear zones they dissect. As a result, strike-slip shear zones should be thinner and less diffuse than zones of deeper-formed dip-slip shear (e.g. Sibson 1977).

Subduction-related strike-slip ductile shear may have been active throughout the history of the TSZ, but older strike-slip zones would have been overprinted by later dip-slip displacement. Dextral movement within the western L_{ss} domain dominantly outlasted dip-slip motion, and was therefore preserved recording lower metamorphic pressures and temperatures than tectonites formed during dip-slip movement. The TSZ may thus preserve a record of late Paleozoic–early Mesozoic oblique convergence and subduction with progressive kinematic evolution from initial dip-slip shear during W-dipping subduction to right-lateral margin-parallel translation along subduction-related strike-slip shear zones.

West-dipping (present co-ordinates) oblique subduction beneath the arc would result in closure of the basin separating the E-facing arc from the North American continental margin. Present data do not indicate the size of such a basin. With final basin closure the subduction complex and associated arc terrane were thrust eastward onto the North American continental margin in early Jurassic time, locally imbricating the margin itself as recorded by top-to-the-east ductile shear within the peraluminous orthogneiss assemblage. Collision and E-directed thrusting would result in uplift and fast cooling of subduction zone tectonites and arc terrane, whereas the overthrust continental margin would be synchronously buried. Top-to-the-east ductile shear recorded in peraluminous orthogneiss of the footwall is interpreted as having formed during collision and terrane accretion. North American continental margin strata were uplifted slowly during late Jurassic to mid-Cretaceous time following early Jurassic terrane accretion. In the late Cretaceous, TSZ tectonites within the hangingwall were juxtaposed with footwall tectonites along a ductile dextral shear zone. In addition, the region was intruded by late Cretaceous plutons and locally disrupted by steep, NNW-trending faults such as the Big Salmon, Teslin and d'Abbadie faults.

CONCLUSIONS

In summary, the TSZ represents a zone of penetrative ductile deformation formed under moderately high-P–T conditions. Tectonic movement within the TSZ began parallel to a steeply-plunging, W-trending lineation (L_{ds}) at a high angle to the ancient plate margin, along which both normal and reverse motion are recorded. Later movement evolved into right-lateral translation (L_{ss}) parallel to the margin along a shear zone which formed subparallel to the material anisotropy of previously-formed structural fabrics. These structures probably formed within the convergent environment of an oblique subduction system. L_{ds} dip-slip displacement may record downflow and return flow within a subduction channel as material from the channel was underplated to the overriding plate. L_{ss} shear zones are interpreted to represent subduction-related strike-slip faults which formed prior to final terrane accretion. Finally, the entire ductilely-deformed tectonite package was imbricated and thrust onto North American cratonal strata along ENE-directed thrusts.

Acknowledgements—This work was supported by the Exploration and Geological Services Division of DIANA, Whitehorse, Yukon, by

National Science Foundation Grant (EAR85-07953) to W. G. Ernst and V. L. Hansen, and by the Department of Earth and Space Sciences, University of California, Los Angeles, in the form of a graduate research fellowship. Many people have contributed to my understanding in the way of discussions; in particular I thank M. Barton, P. Choukroune, W. G. Ernst, J. Goodge, B. Hacker, B. Hanson and D. Kemp. B. Cieutat assisted me in measuring quartz c-axes. J. M. Christie, W. G. Ernst and J. W. Goodge improved preliminary versions of this manuscript; two anonymous reviewers also greatly shortened and improved this paper. All errors or misinterpretations remain my responsibility.

REFERENCES

Aleinikoff, J. N., Dusel-Bacon, C. & Foster, H. L. 1986. Geochronology of augen gneiss and related rocks, Yukon–Tanana terrane, east-central Alaska. *Bull. geol. Soc. Am.* **97**, 626–637.

Aleinikoff, J., Dusel-Bacon, C., Foster, H. L. & Futa, K. 1981. Proterozoic zircon from augen gneiss, Yukon–Tanana Upland, east-central Alaska. *Geology* **9**, 469–473.

Armstrong, R. A. 1988. Mesozoic and Early Cenozoic magmatic evolution of the Canadian Cordillera. In: *The Rogers Volume.*

Arthaud, F. 1969. Méthode de détermination graphique des directions de raccouissement d'allongement et interédiaire d'une population de faille. *Bull. Soc. géol. Fr.* **11**, 729–737.

Beck, M. E., Jr. 1986. Model for late Mesozoic–early Tertiary tectonics of coastal California and western Mexico and speculations on the origin of the San Andreas fault. *Tectonics* **5**, 49–64.

Behrmann, J. H. & Platt, J. P. 1982. Sense of nappe emplacement from quartz c-axis fabrics; an example from the Beltic Cordilleras (Spain). *Earth Planet. Sci. Lett.* **59**, 208–215.

Bell, T. H. 1978. Progressive deformation and reorientation of fold axes in a ductile mylonite zone: the Woodroffe thrust. *Tectonophysics* **44**, 285–320.

Bell, T. H. & Hammond, R. L. 1984. On the internal geometry of mylonite zones. *J. Geol.* **92**, 667–686.

Bennett, V. C. & Hansen, V. L. 1988. Neodymium isotopic similarities between the Yukon–Tanana Terrane, Yukon Territory and continental North America. *Geol. Soc. Am. Abs. w. Prog.* **20**, A111.

Berthé, D., Choukroune, P. & Jégouzo, P. 1979. Orthogneiss, mylonite and non-coaxial deformation of granite: the example of the South Armorican shear zone. *J. Struct. Geol.* **1**, 31–42.

Bryant, B. & Reed, J. C. 1969. Significance of lineation and minor folds near major thrust faults in the southern Appalachians and the British and Norwegian Caledonides. *Geol. Mag.* **106**, 412–429.

Choukroune, P. 1971. Contribution a'létude des mechanisms de la déformation avec schistositié grace aux cristallisation syncinématiques dans les "zones abritées" ("pressure shadows"). *Bull. Soc. géol. Fr.* **7**, 257–271.

Christie, J. M. 1963. The Moine thrust zone in the Assynt region, Northwest Scotland. *Univ. Calif. Publs geol. Sci.* **40**, 345–439.

Churkin, M., Jr, Foster, H. L., Chapman, R. M. & Weber, F. R. 1982. Terranes and suture zones in east-central Alaska. *J. geophys. Res.* **87**, 3718–3730.

Cloos, M. 1982. Flow melanges: numerical modeling and geologic constraints on their origin in the Franciscan subduction complex, California. *Bull. geol. Soc. Am.* **93**, 330–345.

Coney, P. J., Jones, D. L. & Monger, J. W. H. 1980. Cordilleran suspect terranes. *Nature* **188**, 329–333.

Copeland, P., Hodges, K. V., Harrison, T. M., LeFort, P. & Pecher, A. 1988. Rapid Pliocene uplift associated with the Main Boundary thrust, Central Nepal. *Geol. Soc. Am. Abs. w. Prog.* **20**, A321.

Cowan, D. S. 1985. Structural styles in Mesozoic and Cenozoic mélanges in the western Cordillera of North America. *Bull. geol. Soc. Am.* **96**, 451–462.

Cowan, D. S. & Silling, R. M. 1978. A dynamic, scaled model of accretion at trenches and its implications for tectonic evolution of subduction complexes. *J. geophys. Res.* **83**, 5389–5396.

Dusel-Bacon, C. In press. Metamorphic history of Alaska: Yukon–Tanana Upland and Alaska Range north of McKinley and Denali faults. DNAG volume.

Dusel-Bacon, C. & Aleinikoff, J. 1985. Petrology and tectonic significance of augen gneiss from a belt of Mississippian granitoids in the Yukon–Tanana terrane, east-central Alaska. *Bull. geol. Soc. Am.* **96**, 411–425.

Eisbacher, G. H. 1970. Deformation mechanisms of mylonitic rocks and fractured granites in Cobequid Mountains, Nova Scotia, Canada. *Bull. geol. Soc. Am.* **81**, 2009–2020.

Erdmer, P. 1985. An examination of the cataclastic fabrics and structures of parts of Nisutlin, Anvil and Simpson allochthons, central Yukon: test of the arc–continent collision model. *J. Struct. Geol.* **7**, 57–72.

Erdmer, P. & Helmstaedt, H. 1983. Eclogite from central Yukon: a record of subduction at the western margin of ancient North America. *Can. J. Earth Sci.* **20**, 1389–1408.

Etchecopar, A. & Malavieille, J. 1987. Computer models of pressure shadows: a method for strain measurement and shear sense determination. *J. Struct. Geol.* **9**, 667–678.

Fitch, T. J. 1972. Plate convergence, transcurrent faults, and internal deformation adjacent to Southeast Asia and the western Pacific. *J. geophys. Res.* **77**, 4432–4461.

Foster, H. L., Keith, T. E. C. & Menzie, W. D. 1987. Geology of East-Central Alaska. *U.S. geol. Surv. Open-File* **87-188**, 1–55.

Gabrielse, H. 1986. Major dextral transcurrent displacements along the Northern Rocky Mountain Trench and related lineaments in north-central British Columbia. *Bull. geol. Soc. Am.* **96**, 1–14.

Gordey, S. P. 1981. Stratigraphy, structure and tectonic evolution of southern Pelly Mountains in the Indigo Lake area, Yukon Territory. *Bull. geol. Surv. Can.* **318**, 1–44.

Hansen, V. L. 1986. Metamorphic and structural evidence of a Mesozoic transpressional North American margin. *Geol. Soc. Am. Abs. w. Prog.* **18**, 627.

Hansen, V. L. 1987a. Structural, metamorphic, and geochronologic evolution of the Teslin suture zone, Yukon: evidence for Mesozoic oblique convergence outboard of the northern Canadian Cordillera. Unpublished Ph.D. thesis, University of California, Los Angeles.

Hansen, V. L. 1987b. Tectonic correlation of the Yukon–Tanana (YT) and Slide Mountain (SMT) terranes. *Geol. Soc. Am. Abs. w. Prog.* **19**, 386.

Hansen, V. L. 1989. Mesozoic evolution of the Yukon–Tanana terrane. *Geol. Soc. Am. Abs. w. Prog.* **21**, 90.

Hansen, V. L., Heilzer, M. T. & Harrison, T. M. 1988. Mesozoic thermal evolution of the Yukon–Tanana Terrane, Yukon and Alaska: new evidence from $^{40}Ar/^{39}Ar$ data. *Geol. Soc. Am. Abs. w. Prog.* **20**, A111–A112.

Hansen, V. L., Mortensen, J. K. & Armstrong, R. L. In press. Pre-Jurassic ductile deformation and synchronous metamorphism of the Yukon–Tanana terrane: geochronologic constraints from the Teslin suture zone, Yukon. *Can. J. Earth Sci.*

Howell, D. G. 1985. *Tectonostratigraphic Terranes in the Circum-Pacific region.* Circum-Pacific Council for Energy and Mineral Resources Earth Science Series **1**.

Jones, D. L., Silberling, N. J., Coney, P. J. & Plafker, G. 1984. Lithotectonic terrane map of Alaska (west of the 141st Meridian). In: *Lithotectonic Terrane Maps of the North American Cordillera* (edited by Silberling, N. J. & Jones, D. L.). *U.S. Geol. Surv. Open File* **84-523**, A1–A12.

Karig, D. E., Sarewitz, D. R. & Haeck, G. D. 1986. Role of strike-slip faulting in the evolution of allochthonous terranes in the Philippines. *Geology* **14**, 852–855.

Lister, G. S. & Snoke, A. W. 1984. S–C mylonites. *J. Struct. Geol.* **6**, 617–638.

Lister, G. S. & Williams, P. F. 1979. Fabric development in shear zones: theoretical controls and observed phenomena. *J. Struct. Geol.* **1**, 283–297.

Metcalfe, P. & Clark, G. S. 1983. Rb–Sr whole rock age of the Klondike Schist, Yukon Territory. *Can. J. Earth Sci.* **20**, 886–891.

Monger, J. W. H. & Berg, H. C. 1984. Lithotectonic terrane map of western Canada and southeastern Alaska. In: *Lithotectonic Terrane Maps of the North American Cordillera* (edited by Silberling, N. J. & Jones, D. L.). *U.S. Geol. Surv. Open File* **84-523**, B1–B31.

Mortensen, J. K. 1985. Field relationships, U–Pb ages, and correlation of the meta-igneous rocks in the Klondike district, Yukon–Tanana terrane, west-central Yukon Territory. *Geol. Soc. Am. Abs. w. Prog.* **17**, 371.

Mortensen, J. K. 1988. Significance of episodic magmatism in Yukon–Tanana Terrane, Yukon and Alaska. *Geol. Soc. Am. Abs. w. Prog.* **20**, A111.

Mortensen, J. K. & Jilson, G. A. 1985. Evolution of the Yukon–Tanana terrane: evidence from southeastern Yukon Territory. *Geology* **13**, 806–810.

Nokleberg, W. J. & Aleinikoff, J. N. 1985. Summary of stratigraphy, structure and metamorphism of Devonian igneous-arc terranes, northeastern Mount Hayes quadrangle, eastern Alaska Range. *U.S. Geol. Surv. Circ.* **967**, 66–71.

Platt, J. P. 1983. Progressive refolding in ductile shear zones. *J. Struct. Geol.* **5**, 619–622.

Rhodes, S. & Gayer, R. A. 1977. Non-cylindrical folds, linear structures in the X direction and mylonite developed during translation of the Caledonian Kalak Complex of Finnmark. *Geol. Mag.* **114**, 329–408.

Ridley, J. 1986. Parallel stretching lineations and fold axes oblique to a shear displacement direction. *J. Struct. Geol.* **8**, 647–653.

Roddick, J. A. 1967. Tintina Trench. *J. Geol.* **75**, 23–33.

Schmid, S. M. & Casey, M. 1986. Complete fabric analysis of some commonly observed quartz *c*-axis patterns. In: *Mineral and Rock Deformation: Laboratory Studies—The Paterson Volume* (edited by Hobbs, B. E. & Heard, H. C.). *Am. Geophys. Un. Geophys. Monogr., Maurice Ewing Series* **36**, 263–286.

Shreve, R. L. & Cloos, M. 1986. Dynamics of sediment subduction, melange formation and prism accretion. *J. geophys. Res.* **91**, 10,229–10,245.

Sibson, R. H. 1977. Fault rocks and fault mechanisms. *J. geol. soc. Lond.* **133**, 191–213.

Silberling, N. J. & Jones, D. L. (editors) 1984. Lithotectonic Terrane Maps of the North American Cordillera. *U.S. Geol. Surv. Open File* **84-523**.

Tempelman-Kluit, D. J. 1970. An occurrence of eclogite near Tintina trench, Yukon. *Can. Geol. Surv. Pap.* **70-1B**, 19–22.

Tempelman-Kluit, D. J. 1972. Geology and origin of the Faro, Vangorda, and Swim concordant zinc–lead deposits, central Yukon Territory. *Bull. Can. Geol. Surv.* **208**.

Tempelman-Kluit, D. J. 1976. The Yukon crystalline terrane: enigma in the Canadian Cordillera. *Bull. geol. Soc. Am.* **87**, 1343–1357.

Tempelman-Kluit, D. J. 1977. Quiet Lake (105F) and Finlayson Lake (105G) map area, Yukon. *Can. Geol. Surv. Open File* **486**.

Tempelman-Kluit, D. J. 1979. Transported cataclasite, ophiolite and granodiorite in Yukon: evidence of arc–continent collision. *Can. Geol. Surv. Pap.* **79-14**, 1–27.

Tempelman-Kluit, D. J. 1984. Geology, Laberge (NTS 105E) and Carmacks (115I), Yukon Territory. *Can. Geol. Surv. Open File* **1101**.

Toriumi, M. & Masui, M. 1986. Strain patterns in the Sanbagawa and Ryoke paired metamorphic belts, Japan. *Mem. geol. Soc. Am.* **164**, 387–397.

Turner, F. J. & Weiss, L. E. 1963. *Structural Analysis of Metamorphic Tectonites*. McGraw-Hill, New York.

Wilson, F. H., Smith, J. G. & Shew, N. 1985. Review of radiometric data from the Yukon Crystalline Terrane, Alaska and Yukon Territory. *Can. J. Earth Sci.* **22**, 525–537.